JOURNAL OF MATERIALS SCIENCE 11 (1976) 1653–1660

Acoustic emission in brittle solids

W. E. SWINDLEHURST
Atomenergikommissionens Forsøgsanlaeg Risø, 4000 Roskilde, Denmark

T. R. WILSHAW
Effects Technology, Inc, 5383 Hollister Avenue, Santa Barbara, California, USA

A signal/source correlation study of the stress waves emitted during unstable microscopic Hertzian fracture in glass is described. A theoretical analysis of the variation in excess strain energy with applied load is made and the results compared with experimental data covering a wide range of crack sizes.

1. Introduction

An essential step in the development of the acoustic emission detection technique, both for non-destructive testing applications and as a materials science research tool, is the establishment of a signal/source correlation. Accordingly, in recent years a number of studies [1–14] have been made on a wide variety of materials in an attempt to relate recorded emission data to their source characteristics. However, in all such experiments, a major problem is the choice of material and deformation mode for which the emission source can be readily identified and quantitatively analysed. As a part of a continuing effort in this direction, the investigation presented in this paper is directed towards an understanding of the brittle fracture process and its associated acoustic emission. However, with the above mentioned difficulties in mind, the present experiments were designed using the indentation fracture phenomenon [5] as a controlled microscopic emission source which is amenable to fracture mechanics modelling.

The particular type of indentation fracture used is that caused by the loading of a sphere normally onto a brittle solid surface. Both the stress field and the deformation associated with this indentation geometry are generally known as Hertzian, after Hertz [6] who originally formulated the stress field solution. At a critical stage during the loading of such an indenter, a conically shaped crack (Fig. 1) may be suddenly produced in the region of the contact circle. The fracture is caused by the extension of an already present surface flaw

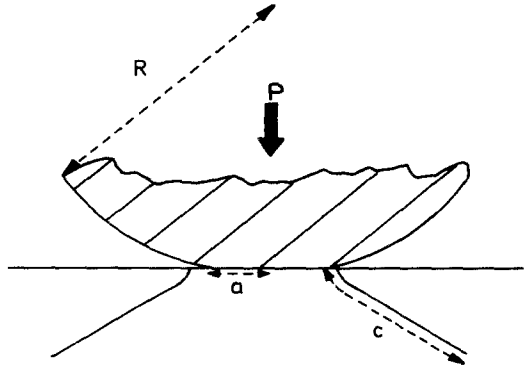

Figure 1 Hertzian indentation geometry: R, indenter radius, a, contact circle radius; c, cone-crack length, P, load on the indenter.

in the highly inhomogeneous subsurface stress field. A further advantage in using this indentation system is that it is being current employed in the study of crack growth in brittle materials [7–10]. In this application, the load at which the crack rapidly devlops is used to quantify the fracture behaviour of the material under investigation. Consequently, the ability to detect crack growth acoustically will find direct application in such investigations.

2. A model for emission behaviour

A method is described for calculating the total excess energy, ΔU_k, which is generated during the growth of a cone crack in a Hertzian stress field created in an ideally brittle solid. This energy comprises the total mechanical energy released during crack growth minus that necessarily re-

quired to propagate the crack. From a mechanistic point of view, ΔU_k will manifest itself as the kinetic energy of the rapidly separating crack walls. A fraction of this energy will then be transmitted into the bulk of the solid in the form of stress waves – detectable as acoustic emission. ΔU_k represents the maximum energy available for conversion into acoustic emission. No attempt is made to calculate the exact fraction so converted.

The system to be studied is an ideally brittle body of unit thickness which is subject to external forces at its boundaries [11]. On the Griffith model, a crack in such a material is assumed to be in equilibrium if $dU_T/dc = 0$, where U_T is the total energy of the system and c the crack length. dU_T/dc considered to be composed of two terms, one involving G, the rate of change of mechanical energy with crack length and the other γ, the specific surface energy of the body

$$dU_T/dc = -G + 2\gamma. \quad (1)$$

If, in addition, d^2U_T/dc^2 is positive, the system is in unstable equilibrium and a finite increase Δc in the crack length results in a decrease in U_T.

$$\Delta U_T = -G\Delta c + 2\gamma\Delta c < 0. \quad (2)$$

Thus, excess energy, ΔU_k, is released beyond that required for crack extension. To account for the presence of this energy in the system we may write

$$-G\Delta c + 2\gamma\Delta c + \Delta U_k = 0. \quad (3)$$

Accordingly, this excess energy released during crack growth from c_1 to c_2 may be written as

$$\Delta U_k = \int_{c_1}^{c_2} G dc - 2\int_{c_1}^{c_2} \gamma dc \quad (4)$$

where ΔU_k has the units of energy per unit thickness. To include the possibility of a variable crack front width, L, the above equation becomes

$$\Delta U_k = \int_{c_1}^{c_2} GL dc - G_c \int_{c_1}^{c_2} L dc \quad (5)$$

where $G_c = 2\gamma$ and ΔU_k has now absolute units of energy. This equation is generally applicable to unstable fracture situations in brittle materials Specific forms of the equation have been described in the literature using expressions for G and L appropriate to the particular testing configurations employed, for example Gerberich and Hartbower [12] use $G = \pi\sigma^2 c/E$ (where σ is the tensile stress on the specimen and E Young's modulus) and a constant L. Under these conditions the first term in Equation 5 can be easily evaluated analytically.

However, because of the highly inhomogeneous nature of the Hertzian stress field, G in this case has to be analysed numerically as a function of c. This calculation has been performed by Lawn [13] and Frank and Lawn [14] for crack growth initiating from the edge of the contact circle. An extension of this analysis has been made by Wilshaw [7] for cracks initiating beyond the edge of the contact circle edge. In all these analyses, G is usually represented as a function of c in normalized co-ordinates, $-G/G_c$ as a function of c/a (the instantaneous crack length normalized to the instantaneous value of the contact circle radius, a). An example of such a diagram, after Wilshaw [7] is given in Fig. 2a.

These curves can be used to provide a semi-quantitative insight into the relative amounts of excess energy released during cone growth under different conditions. For unit width of crack front, Equation 5 can be written as

$$\Delta U_k/G_c = \int_{(c/a)_1}^{(c/a)_2} a(G/G_c)d(c/a) - \int_{(c/a)_1}^{(c/a)_2} a\,d(c/a) \quad (6)$$

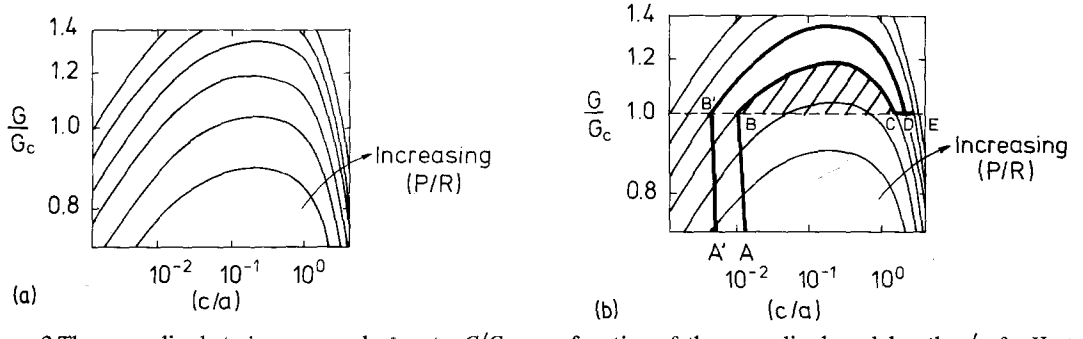

Figure 2 The normalized strain energy release rate, G/G_c, as a function of the normalized crack length, c/a, for Hertzian cone fracture.

or, because a is effectively constant over the fast crack growth regime being considered here,

$$\Delta U_k/G_c = a\left[\int_{(c/a)_1}^{(c/a)_2}(G/G_c)\mathrm{d}(c/a) - \left\{\left(\frac{c}{a}\right)_2 - \left(\frac{c}{a}\right)_1\right\}\right]. \quad (7)$$

The function within the outer brackets in Equation 7 is shown as the shaded area in Fig. 2b This region represents ΔU_k released during the cone growth described by the line ABCDE. However this area is *not* an quantitative measure of ΔU_k because Equation 7 is only valid for unit width of crack front. AB'D'E describes crack growth at a greater fracture load, P_F. It can clearly be seen that the corresponding value of ΔU_k is larger.

To obtain an accurate quantitative estimate of ΔU_k for the Hertzian cone fracture, Equation 5 must be evaluated numerically. Such a calculation has been performed using the computer program developed by Lawn, *et al.* [15]. The three-dimensional expansion of the cone crack was accounted for by the use of the appropriate value of L at each successive crack-step increment. In order to compare the theoretical results with the experimental data (Section 3), experimental conditions were simulated in terms of the environmental reactivity and a suitable time to fracture. The assumptions implicit in the program are described in the reference cited. In addition to these, for the present application it was not possible to define the exact initial flow conditions. This was because the experimental data were obtained using polished glass surfaces. An accurate simulation would then have required the statistical surface flow distribution to be incorporated into the program. This was not possible because of both the uncertainty in the exact flow distribution function, and the computer time required. To overcome this difficulty, the program was "fitted" to the experimental data by using an initial surface flow depth which gave fracture loads comparable to the experimental data, for similar indenter sizes. A submicon (0.15 μm) flaw depth was used, together with a G_c value of 7.8 J m^{-2} [16].

Output data from these calculations are shown in Fig. 3. ΔU_k is presented as a function of P_F for three indenter sizes. It can be seen that for both environments, a general relationship of

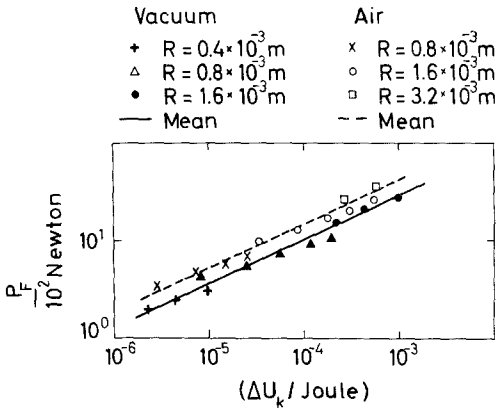

Figure 3 A theoretical estimate of the total energy, ΔU_k, available for acoustic emission as a function of the load, P, on the indenter of fracture. The calculation is made for various indenter radii, R.

the form

$$\Delta U_k \propto (P_F)^n \quad (8)$$

exists, where n is approximately equal to 2.

This predicted dependence of ΔU_k on P_F can be investigated experimentally, providing that the input energy, ΔU_k, to the detection system is a constant fraction of ΔU_k. $\Delta U_k'$ may itself be calculated from the relationships [17]

$$\Delta U_k' \propto V_0^2 \quad (9)$$

and

$$V = V_0 \exp(-\mu N) \quad (10)$$

where V_0 is the initial transducer output voltage and N the experimentally measured emission count. Equation 10 describes the envelope decay curve of the transducer output voltage. A method of measuring μ is described in Section 3.

3. Experimental details

The specimen material was soda-lime glass in the form of 50 x 100 x 10 mm glass blocks which were cut from larger pieces. The largest specimen surfaces were in a polished condition and were prepared for indentation by cleaning in acetone. A diagram of the mechanical testing arrangement is shown in Fig. 4. Each specimen was acoustically isolated from its support by a thin layer of rubber bonded to the specimen by self-adhesive tape. All Hertzian tests were performed at a cross-head descent rate of 8.10^{-6} msec^{-1}, using tungsten carbide indenters of 1.0, 2.0 and 4.0 mm diameter. The test environment was either 25% r.h. air or nitrogen gas (5 ppm H_2O). No indentation was

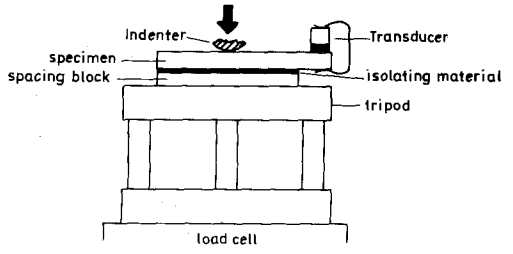

Figure 4 A diagram of the mechanical testing arrangement for acoustic emission studies.

performed closer than 10 surface ring crack diameters to any other. During testing, the development of the cone crack could be observed through the longer specimen sides using a travelling microscope. For this purpose the face was ground and polished before the experiment was begun. Measurement of thefinal cone dimensions were made only on indentations produced in the nitrogen environment, while the indenter was held at fracture load. The first condition prevented possible inaccuracies due to stress corrosion-aided slow crack growth and the second, inaccuracies due to "optical crack healing" of the cone. After complete indentation of a specimen the surface traces of the fractures were made visible by etching in a 4% HF solution for 30 sec.

Mechanical/electrical acoustic signal conversion was performed by a commercial piezoelectric transducer*. The transducer was acoustically coupled to the specimen with a thin layer of silicon vacuum grease. The transducer output was fed into processing equipment consisting of a wide band pre-amplifier, a narrow band (100 to 300 kHz) main amplifier and a variable voltage level detector†. The detector enabled the strength of each acoustic signal to be measured by counting the number N, of transducer resonance oscillations above a fixed voltage reference level. This method of signal analysis is known generally as "ring-down" counting [18]. The final signal voltage was then fed into a pen-recorder using a digital to analogue converter. For these experiments the system gain was fixed at 75 dB and the threshold voltage at 1 V.

The decay constant,U, in Equation 5 was measured by using a constant strength single pulse emission source on a sample specimen block. This was supported in the same manner as those used for the indentation experiments, to prevent variations in the damping characteristics. N was then measured as a function of the gain of the detection system. The artificial source used was a 5×10^6 Hz resonant frequency quartz crystal excited by an input voltage step with a rise time of 3×10^{-6} sec. This was of a similar time duration to that of the fracture emission pulse [19].

4. Results

Fig. 5 shows typical features of the surface traces of Hertzian cone cracks, together with the corresponding load/time and cumulative emission/time curves. It was found that emission occurring prior to cone formation was substantially reduced by careful acoustic isolation of the specimen. Accordingly this was attributed to noise generated during the seating of the loading system.

The complexity of the emission associated with indentation reflected the complexity of the surface fracture trace. A single Hertzian cone crack produced a single emission burst (Fig. 5a). If additional fracturing occurred (Fig. 5b), then further emission bursts were recorded. These were produced after the development of the initial cone crack. For each indenter size, the multiple fractures similar to Fig. 5b were produced at higher fracture loads, the approximate transition load increasing with increasing indenter size. It was also found that any emission generated during the unloading of the indenter was associated with secondary cone growth (Fig. 5c).

The experimentally measured strength, N, of the emission associated with cone growth is presented as a function of the fracture load P_F, and the final cone length, c_L, in Fig. 6. It can be seen that neither the test environment nor the indenter size have any effect on the near N/P_F or N/c_L relationships as represented by the solid lines in the figures. Because of limitations on the artificial source strength, the decay constant, μ, was measured only for the lower half of the data in Fig. 6. This value of μ was then used to calculate values of $\Delta U'_k$ according to Equations 9 and 10. These results are presented in Fig. 7. The datum limits in this figure were calculated using an approximate data spread indicated by the arrow in Fig. 6b. For the purpose of com-

* Dunegan/endevco D 140 B.

† A.I.M. Electronics.

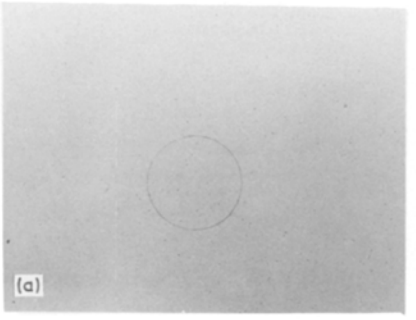

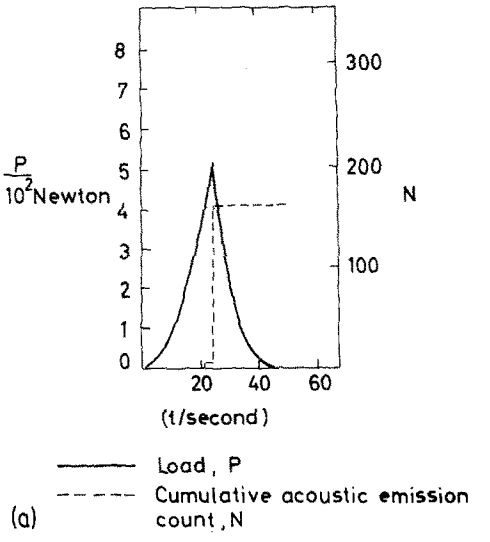

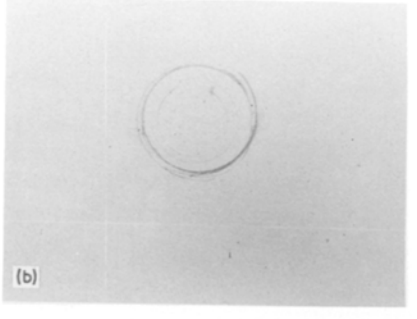

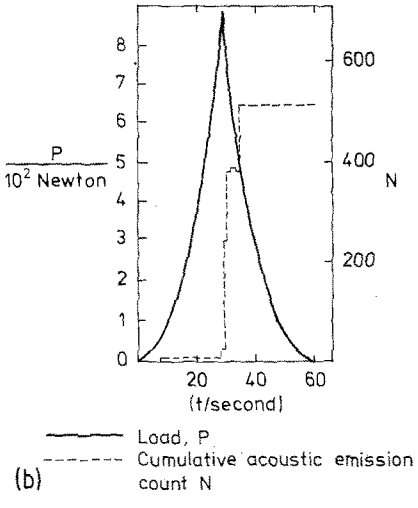

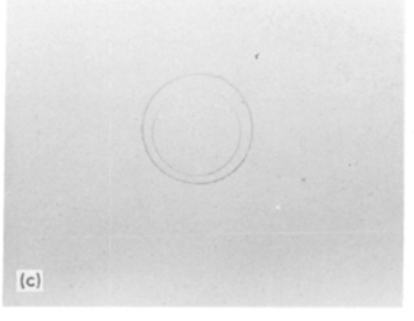

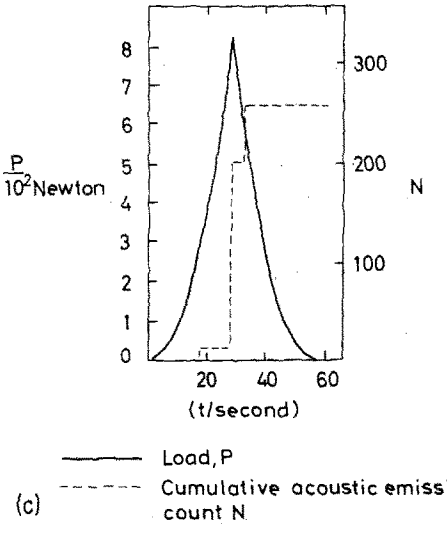

Figure 5 Surface traces of typical Hertzian cone cracks, together with load and emission curves.

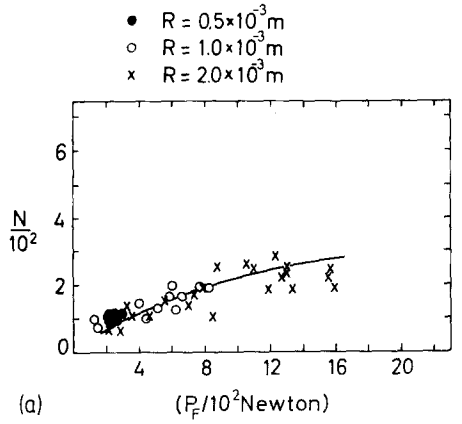

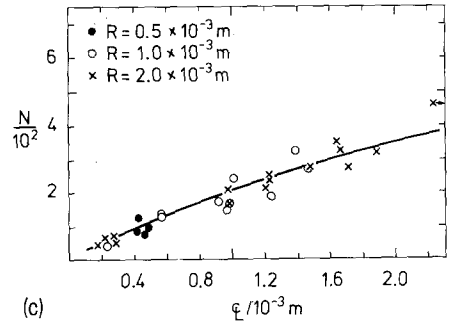

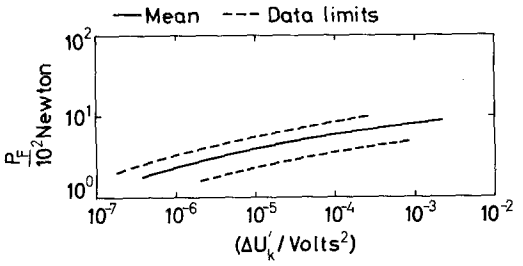

Figure 7 The experimentally measured acoustic emission strength, $\Delta U_k'$, in the form of initial transducer voltage, as a function of the fracture load, P_F.

parison with the theoretical predictions of Fig. 3, the mean U_k' curve can be approximated to by the equation

$$\Delta U_k' \propto (P_F)^n$$

where n equal 5.5.

5. Discussion

The ability of acoustic emission techniques to detect the development of Hertzian cone fracture has been demonstrated. In particular, the acoustic detection of crack growth assumes importance when either the fracture is invisible (due to its size or opaque specimen material) or, in static fatigue

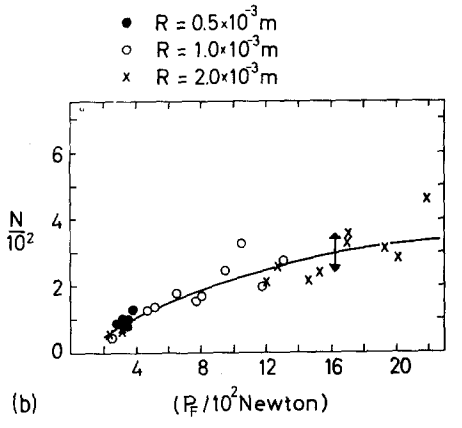

Figure 6 The experimentally measured acoustic emission counts, N, from Hertzian cone crack growth as a function of the load, P_F, at fracture, or cone crack length, C_L. (a) Air environment, (b) and (c) nitrogen.

studies where continuous specimen observation is not possible. It must be emphasized that precautions need to be taken to minimize the acoustic noise generated by the loading system. The results described above apply specifically to Hertzian crack growth initiating from polished surfaces. Further considerations, applicable to other materials and surface conditions will be made below.

Discussion about the quantitative aspects of acoustic emission measurements can most easily be made with reference to Figs. 3 and 7. The experimental independence of N of indenter size and environment agrees with the theoretical calculations, within the spread of the experimental data. Conversely, on the assumption that $\Delta U_k'$ is proportional to ΔU_k, there is a marked difference between the experimental and the calculated values of the exponent in Equation 8. It is not possible to state definitively whether or not this discrepancy indicates that $\Delta U_k'$ is not proportional to ΔU_k, because the spread in experimental data does not allow the mean V_0^2/P_F curve to be specified accurately enough to draw such a conclusion. It is most probable that this spread is due to the difficulty in separating the emission generated by cone growth from that produced by the additional fracturing (Fig. 5b). The multiple cracking itself resulting from the high fracture loads associated with the Hertzian indentation of polished glass surfaces. This experimental/theoretical discrepancy will also exist for the N/c_L measurements. This is because the $P_F^2 \propto c_L^3$ relationship [20], theoretically valid for the fully developed cone was found to hold experimentally.

In conclusion, it is useful to discuss the limits of applicability of the model described above. The second term in Equation 5 represents the energy which is necessary to propagate a crack a distance $(c_2 - c_1)$. It is presumed that this energy does not activate any detectable emission sources which may lie within a "process zone" around the crack tip. The linear dimension of this region is defined approximately as

$$\Gamma = \frac{GE}{2\Pi\sigma_y}$$

for low applied stress levels, where σ_y is the yield stress of the material and E is the Young's modulus. An estimated value of Γ for silicate glasses is so small that the assumption is probably valid. On the other hand, for materials where Γ is larger, microcracking [21] or plastic deformation [22] within this region may well give rise to emission. Accordingly, the present model, which is applicable to ideally brittle solids, would have to be extended to included crack tip plasticity effects.

A further important limitation of the present model is that it applies to brittle fracture situations where crack growth is both macroscopically and microscopically continuous, as for example in homogeneous brittle materials such as silicate glasses. The energetics of crack growth only are considered, excess energy which manifests itself as the kinetic energy of the rapidly separating crack walls, being generated when $G > G_c$. A proportion of the energy is then transmitted into the bulk of the solid as stress waves, recordable as acoustic emission. Thus, continuous crack growth would not be expected to generate detectable acoustic emission [23, 24] because of the low energy release rate. According to the present model no energy is available for emission when G falls to become equal to G_c. Consequently, although slow crack growth is not considered explicitly, it is considered implicitly, because a choice of a value of G_c implies, from standard crack velocity/G data [15] a minimum velocity below which emission is not generated. In the absence of any experimental data the choice of G_c becomes rather arbitrary. With reference to Fig. 2b, the variation in G_c reflects itself as a variation in the position of the $G/G_c = 1$ broken line. This results in a variation in the absolute value of ΔU_k. Consequently, the present study was limited to an investigation of polished glass surfaces where, because of the Hertzian stress field configuration, the small effective surface flaw depth gives rise to only a minimal amount of initial slow crack growth. In addition, the independence of the experimental data of the environment indicates that no significant unpredicted environmentally assisted slow crack growth effects were produced.

The above discussion has been limited to homogeneous brittle materials. As an example of discontinuous slow crack growth emission, crack extension in structural ceramics [21] has been found to be acoustically detectable even when the macroscopic growth rate is as low as 10^{-6} msec^{-1} ($G = G/3$ for fast crack growth). This emission is presumed to be due to the discontinuous microscopic nature of the crack development, bursts of fast extension occurring when the crack front jumps between successive pinning points. It would, therefore, be expected that the indentation emission characteristics would be different from those described above, in that slow crack growth both prior to and after cone development would give rise to acoustic emission.

Acknowledgements

This work was carried out at the Material Science Laboratories of The University of Sussex, England. Financial support was provided by The British Glass Industries Research Association, Sheffield and United Glass Limited, St. Albans.

References

1. K. N. TANDON and K. TANGRI, *Mat. Sci. Eng.* **20** (1975) 47.
2. M. MIRABILE, *Non-dest. Test.* April (1975) 77.
3. R. PASCUAL, M. AHLERS, R. PAPACIOLI and W. ARNEODO, *Scripta Met.* **9** (1975) 79.
4. R. T. SEDGWICK, *J. Appl. Phys.* **39** (1968) 1728.
5. B. LAWN and R. WILSHAW, *J. Mater. Sci.* **10** (1975) 1049.
6. H. HERTZ, "Hertz miscellaneous papers" (Macmillan, London, 1896) Ch. 5.
7. T. R. WILSHAW, *J. Phys. D. Appl. Phys.* **4** (1971) 1567.
8. F. B. LANGITAN and B. R. LAWN, *J. Appl. Phys.* **41** (1970) 3357.
9. B. R. LAWN, T. R. WILSHAW, T. E. BERRY and R. MORELL, *J. Mater. Sci.* **10** (1975) 179.
10. Y. M. TSAI and H. KOLSKY, *J. Mech. Phys. Solids* **15** (1967) 29.
11. B. R. LAWN and T. R. WILSHAW "Fracture of Brittle Solids" (Cambridge University Press, 1975).
12. W. W. GERBERICH and C. E. HARTBLOWER, *Int. J. Fract. Mech.* **3** (3) (1967) 185.

13. B. R. LAWN, *J. Appl. Phys.* **39** (1968) 4828.
14. F. C. FRANK and B. R. LAWN, *Proc. Roy. Soc. A* **229** (1967) 291.
15. B. R. LAWN, T. R. WILSHAW and N. E. W. HARTLEY, *Int. J. Fract.* **10** (1974) 1.
16. S. M. WIEDERHORN, *J. Amer. Ceram. Soc.* **52** (2) (1969) 99.
17. D. O. HARRIS, A. S. TETELMAN and F. A. DARWISH, A.S.T.M S.T.P. 505 A.S.T.M. (1972) p. 238.
18. B. J. BRINDLEY, J. HOLT and I. G. PALMER, *Non-dest. Test.* December (1973) 299.
19. Y. M. TSAI and H. KOLSKY, *J. Mech. Phys. Solids* **15** (1967) 263.
20. F. C. ROESLER, *Proc. Roy. Soc. B* **69** (1956) 981.
21. A. G. EVANS and M. LINZER, *J. Amer. Ceram. Soc.* **56** (11) (1973) 575.
22. K. ISHIKAWA and H. C. KIM, *J. Mater. Sci.* **9** (1974) 737.
23. I. S. GUZ and V. M. FINKEL, *Sov. Phys. Solid Stat.* **14** (1973) 1619.
24. J. D. BYERLEE and L. PESELNICK, *Naturwiss.* **57** (1970) 82.

Received 23 January and accepted 23 February 1976.